

Infinitesimal Drift Diffeomorphometry Models for Population Shape Analysis

Brian C. Lee¹, Daniel J. Tward¹, Zhiyi Hu¹, Alain Trouvé², Michael I. Miller¹

¹Johns Hopkins University, Baltimore, MD, USA

²Université Paris-Saclay, ENS Paris-Saclay, CNRS, Centre Borelli, F-94235, Cachan, France

¹{leebc, dtward, zhiyi, mim}@cis.jhu.edu, ²trouve@cmla.ens-cachan.fr

Abstract

Describing longitudinal morphometric differences between populations and individuals is a critical task in computational anatomy. In the context of the random orbit model of computational anatomy, this often implies study of the variation of individual shape trajectories associated to some mean field, as well as longitudinal morphological differences as encoded by similar subjects from representative populations. In this paper, we present a new method for computing the deviation of individual subjects from models of flow. We demonstrate estimation of the infinitesimal drift representing the mean flow of a population and its entrance into the Eulerian vector field controlling that flow. Each individual is studied longitudinally by modeling another associated individual drift which acts as the personalized control of the flow. We provide an augmentation of the classic LDDMM equations to generate "biased geodesics" for trajectory shooting algorithms, allowing for direct computation of the individual's deviation under the influence of a mean drift. Our new model is inspired by diffusion models from stochastic processes in which the personalized control is a non-stochastic term representing the additive Brownian component on top of the infinitesimal drift representing the population. We present results of our model on entorhinal cortical surfaces extracted from a patient population of the Alzheimer's Disease Neuroimaging Initiative.

1. Introduction

The use of diffeomorphic mapping in computational anatomy has been extremely successful in the longitudinal and cross-sectional study of shape and structure. The basic model employed is that the space of shapes $I \in \mathcal{I}$ is an orbit acted on by the group of diffeomorphisms $\varphi \in \text{Diff}$, where the orbit is generated by the group action $\mathcal{I} \doteq \{\varphi \cdot I, , \varphi \in \text{Diff}\}$ [19, 28]. Typically the shape I can be a dense image [7], sets of landmarks [23], or surfaces and currents [44, 13] with and without correspondences.

Diffeomorphic flows are controlled by the evolution

$\dot{\phi}_t = v_t \circ \phi_t, t \in [0, 1]$ with $\varphi \doteq \phi_1$ for smooth vector fields $v \in V$ in a smooth reproducing kernel Hilbert space, ensuring that the flows are diffeomorphisms [12, 41]. As well, atrophy and growth have been studied for understanding cohorts of shapes under transformation [31], in which time plays a role in simulation time for generating diffeomorphisms as well as in understanding the space-time phenomena of developmental and degenerative disease [10, 11, 47, 46, 45, 38, 9, 37, 25, 5, 4]. This field has progressed quickly and numerous groups have mapped populations of anatomical structures to common coordinate spaces in multiple contexts. These mappings have been studied largely using mixed-effects modeling with statistical permutation testing [43, 40, 30, 48] or linear operations on parameterized deformation fields [36, 2, 35, 26, 42, 39]. The motivation is to understand the typical representative shape change of populations as well as to make decisions concerning large deviations away from typical shape.

At the same time, the representation of population statistics in terms of high dimensional shape models has lagged behind. The mentioned examples have described methods for encoding means and variances of mapped populations in low dimensional statistical representations. However, little work has been done on directly encoding diffeomorphic modeling with typical population shape. The work proposed here is motivated by this goal. We explicitly define the population shape as represented by the mean vector field encoding the flow of the cohort, and we associate to each individual in the population a deviation encoding another personalized vector field. Viewing the diffeomorphism as the state in a dynamical system, then the typical flow encodes the overall average control; the individual is encoded by the deviation via an additional personalized control. These high dimensional trends directly encode typical growth, atrophy, and disease. We embed into our new algorithms both the estimation of the vector field common to the population and the estimation of the per-subject deviation.

In describing the model, we use the language of diffusion and stochastic differential equations studied in the classical stochastic process literature of Brownian motion with drift

[24]. We appreciate that in our setting, the state is infinite dimensional. The infinitesimal drift in our model is the differential change in state given by the diffeomorphic flow; we associate the mean flow or "mean drift" representing the population to the infinitesimal mean of Brownian motion, and likewise associate the personalized infinitesimal motion or "personalized control" to the infinitesimal variance. Our personalized deviation is not stochastic, but is another deterministic drift term replacing the explicit Brownian term. Holm [20] has examined diffeomorphic flows in the context of the stochastic term in this infinite dimensional setting.

Our focus on the infinitesimal mean to encode the population of typical shape as a method to study individual deviations is motivated by the success of representing population means in machine learning and data science. The conditional mean as an estimator is remarkably efficient and ubiquitous. Examples abound in the literature for representation of the expected value of moments via the use of maximum entropy models for speech and image representation [21, 22, 6, 3, 15, 29, 8, 49]. In stochastic optimization and random sampling for inference in high dimensional spaces, the drift term has seen many successful applications by guiding a process towards a particular set of explanations as represented by the posterior distribution [17, 16, 18]. Our representation is also reminiscent of the principles embedded in the usual mixed-effects modeling of lower dimensional statistics. Our goal is to build both the typicality of shape as represented by the population mean and the variance of the individual associated to the individual deviation element into the diffeomorphic flow model itself.

In this work, we present a new model for computing the deviation of individual subjects from the infinitesimal mean drift. We introduce an augmentation of the classic geodesic shooting algorithm to generate what we term "biased geodesics", which allows direct computation of the personalized control under the influence of some flow associated to a population drift term. This deviation can represent intra- or inter-population comparisons. We illustrate methods for computing the mean drift of a population of shapes following neurodegeneration associated to Alzheimer's disease in a common coordinate space by mapping the longitudinal flows using large deformation diffeomorphic metric mapping (LDDMM) parameterized by initial momentum whose coordinate systems can be changed via coadjoint transport. The results of our model are presented associated to a significant cohort in the Alzheimer's Disease Neuroimaging Initiative study.

2. Drift Model for Longitudinal Shape Analysis

Our basic model for longitudinal shape is a mechanodynamic system in which structures are viewed as being embedded in a condensed matter continuum where advection and transport hold [19, 1, 28]. In the following text,

we will refer to the infinitesimal mean as the **mean drift** and the individual deviation as the **personalized control** for simplicity. The model of dynamics for a given subject i is a dense space-time flow of the state $t \rightarrow \varphi_t^{(i)}(x) \in \mathbb{R}^3, x \in \mathbb{R}^3$ with control $t \rightarrow v_t^{(i)}$ given as the superposition of drift $\mu_t^{(i)}(\cdot)$ representing typicality and personalized or individual mechano-dynamics $w_t^{(i)}(\cdot)$:

$$\frac{d\varphi_t^{(i)}}{dt}(x) = v_t^{(i)} \circ \varphi_t^{(i)}(x), \quad \varphi_0^{(i)}(x) = x \quad (1a)$$

$$\text{with } v_t^{(i)} = \mu_t^{(i)} + w_t^{(i)} \quad (1b)$$

where the mean drift μ_t in an exemplar coordinate system (see Figure 1) is transported into the coordinate system specific to subject i to produce $\mu_t^{(i)}$, and $w_t^{(i)}$ is the personalized control. The Eulerian vector fields $v_t^{(i)} \in \mathbb{R}^3$ are modeled as elements of a Hilbert space of smooth and 1-time differentiable functions of space. In the continuum, this smoothness corresponds to the motions seen for transport and advection as associated to growth and atrophy from millimeter to meso-scale. We model the dense vector fields $v \in V$ as being generated via differentiable scale-space kernels $k(\cdot, \cdot)$ acting on L_2 functions:

$$V = \{v = \int k(x, y)h(y)dy, \|h\|_2^2 = \int |h|^2 dx < \infty\}. \quad (2)$$

A diagram of the proposed generative model is displayed in Figure 1. The model is similar to that proposed in [14] in which there is a normalization of each individual flow of the population relative to the template which essentially defines the initial condition of each individual flow, denoted as $\Phi^{(i)}, i = 1, \dots, N$. To define the mean flow of the normalized population within each individual's time series, we coadjointly transport [32] it and denote it as $\mu_t^{(i)}, i = 1, \dots, N$.

2.1. Estimating Personalized Control under Drift

The dynamics space is huge. We select the parsimonious ones based on what we term "biased geodesic flow" via Hamilton's principle and the principle of least action. We term it biased due to the addition of an infinitesimal mean drift representing the population statistics to the standard geodesic equations of LDDMM. We adopt a Hamiltonian control systems model for flows of human anatomy [33]. Given the mean drift $\mu_t^{(i)}$ in an individual's coordinates, we define the Hamiltonian of our dynamical system:

$$H(p, \varphi^{(i)}, w^{(i)}, t) = \int p \cdot ((\mu^{(i)} + w^{(i)}) \circ \dot{\varphi}^{(i)}) dx - \frac{1}{2} \|w^{(i)}\|_V^2 \quad (3)$$

where $\dot{\varphi}^{(i)} = (\mu^{(i)} + w^{(i)}) \circ \varphi^{(i)}$ is a dynamical constraint, and p is termed the Hamiltonian momentum acting as a Lagrange multiplier on the constraint. Our dynamical systems

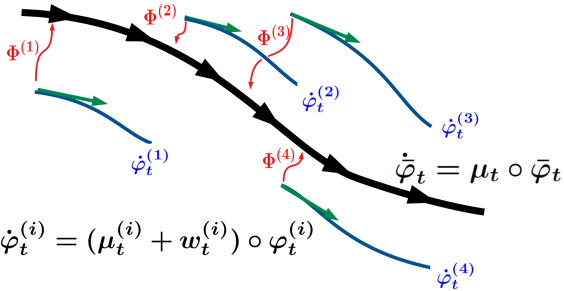


Figure 1. Diagram of infinitesimal mean drift model. The black curve represents the flow generated by the population mean drift μ_t , while individual subject observations' flows are governed by $\dot{\varphi}_t^{(i)}$. The red curve represents transport $\Phi^{(i)}$ of the personalized controls $w_t^{(i)}$ into the coordinate space of the mean drift.

model becomes the following:

$$\begin{aligned}\dot{\varphi}_t^{(i)} &= (\mu_t^{(i)} + w_t^{(i)}) \circ \varphi_t^{(i)} \\ \dot{p}_t^{(i)} &= -d(\mu_t^{(i)} + w_t^{(i)})^T \circ \varphi_t^{(i)} p_t^{(i)} \\ w_t^{(i)}(\cdot) &= \int K(\cdot, \varphi_t^{(i)}(x)) p_t^{(i)}(x) dx\end{aligned}\quad (4)$$

The initial momentum $p_0^{(i)}$ driving the time-varying velocity field $w_t^{(i)}$ can be computed under this constrained optimization scheme and represents the deviation or personalized control of individual i from the background mean drift $\mu_t^{(i)}$. We model $p_0^{(i)}$ as being initially seeded on a set of k discrete control points $q^{(i)}$ such that $p_0^{(i)}(x) = \sum_k w_k^{(i)} \delta(x - q_k^{(i)})$. Notably, $\mu_t^{(i)}$ does not appear in the regularization term of (3) and thus this formulation does not produce the same $w_t^{(i)}$ as for the more classical LDDMM.

2.2. Surface Matching Algorithm

For the following experiments, we assume that the infinitesimal mean drift μ_t of a given population is generated offline and is transported from the population space to the individual subjects' longitudinal trajectory $\mu_t^{(i)}$, $i = 1, \dots, N$. To estimate the mean drift, we model populations of time series of surfaces S_{t_j} , $t_j \in \{t_1, t_2, \dots, t_m\}$ viewed as longitudinal observations from members of labeled cohorts undergoing disease modeling processes. In our setting, we have triangulated mesh cortical surfaces associated to studies such as ADNI [34]. We use current matching for surfaces [44] as adopted for LDDMM to generate the initial momentum fitting through the time-series [42, 43]. We solve for the variational solutions as an optimal control problem, defining the state $t \mapsto q_t = \varphi_t \cdot S$ and the control $t \mapsto v_t$ satisfying the dynamical equations of (4).

The time series of surfaces enters as input data with matching term given by the smooth energy $U : q_t \rightarrow$

R^+ , $t \in [0, 1]$ which drives the state through the target surfaces with pre-defined mean drift μ_t , $t \in [0, 1]$. We pose the following control problem:

$$\begin{aligned}Control Problem: \\ \dot{\varphi}_t^{(i)} &= (\mu_t^{(i)} + w_t^{(i)}) \circ \varphi_t^{(i)}, \\ q_t^{(i)} &= \varphi_t^{(i)} \circ S_0, \quad q_0^{(i)} = S_0, \\ \min_{v_t, t \in [0, 1]} E(v) &:= \frac{1}{2} \int_0^1 \|w_t^{(i)}\|_V^2 dt + \int_0^1 U_t(q_t^{(i)}) dt.\end{aligned}\quad (5)$$

The Hamiltonian momentum satisfies Eqn. (4) with forces:

$$\dot{p}_t^{(i)} = -d(\mu_t^{(i)} + w_t^{(i)})^T \circ \varphi_t^{(i)} p_t^{(i)} + \frac{\partial U_t^{(i)}}{\partial q}(q_t^{(i)}). \quad (6)$$

The energy U_t , $t \in [0, 1]$ is defined by the current matching norm on surfaces (see Supp. A) denoted as $\|\cdot\|_S$:

$$U_t^{(i)}(q_t^{(i)}) = \sum_{t_j} \delta(t - t_j) \frac{1}{\sigma_m^2} \|q_{t_j}^{(i)} - S_{t_j}^{(i)}\|_S^2. \quad (7)$$

We solve the minimization of this new control problem following the method of matching onto surfaces which has been previously described for this class of problems [28].

2.3. Estimating Mean Drift of a Population

We now describe our method for computing the mean drift μ_t from a population of shapes. Figure 2 depicts the setting for our model assuming two populations, disease and control, each with their own mean drift representing their cohort. More generally, there can be any number of subpopulations. The basic idea is to generate for each subject i 's time-series the optimal momentum $p_{0,sub}^{(i)}$ by geodesic shooting of a single trajectory through a time-series, followed by transport of the trajectory's initial momentum into the common population coordinates where we average the momentum of each of the subjects to generate \bar{p}_0 . Each subject's LDDMM flow and initial momentum is transported into the template coordinate space by computing the diffeomorphism $\Phi^{(i)}$ of the subject time-series onto the population template, and then coadjointly transporting [32] the initial momentum into the template coordinates.

For all experiments shown we assume the time series are synchronized allowing us to average the initial momentum of all subjects transported into population template coordinates. Notably, under our proposed framework, any synchronization can be used with no requirement for temporally overlapped data. For instance, time-varying velocity fields associated to the initial momentum could be transported and averaged at a sampling of corresponding time points to produce μ_t . This would increase the number of estimated dimensions of the model. Based on our current sample size we did not believe it was statistically stable to re-estimate those additional dimensions.

The average momentum \bar{p}_0 encodes the population drift μ_t for which we generate Hamiltonian equations for momentum evolution associated to the principles of least action. To derive the mean drift in subject coordinates we coadjointly transport \bar{p}_0 back to the coordinates of each subject defined by the diffeomorphism $\Phi^{(i)}$ mapping the subject i to population coordinates. The coadjoint transport of any initial momentum seeded on discrete control points along $\Phi^{(i)}$ multiply used above is defined by the following (shown here for transport of \bar{p}_0 into the coordinate space of subject i along $\Phi^{(i),-1}$):

$$\bar{p}_0^{(i)} = D[\Phi^{(i)}]^{-1}(\Phi^{(i)})^T \bar{p}_0([\Phi^{(i)}]). \quad (8)$$

$\Phi^{(i)}$ can be determined in several ways – in our examples, we choose to compute $\Phi^{(i)}$ by mapping the first observation of each subject (for instance the first MRI in a longitudinal series of scans, hereafter termed the "baseline") to the template surface at the corresponding time point in the mean flow. Thus each subject's individual trajectory parameterized by $p_{0,sub}^{(i)}$ lies in the reference frame of the baseline but is seeded at control points corresponding to vertices of the template surface triangulation, ensuring $p_{0,sub}^{(i)}$ exists at corresponding points for all subjects.

Algorithm 1 Estimating Infinitesimal Mean Drift Representing Population Shape

Given: time-series surface $S_t^{(i)}, t \in \{t_1, \dots, t_m\}$ and mappings $\Phi^{(i)}$ to population template, $i = 1, \dots, N$:
Geodesic shoot $p_{0,sub}^{(i)}$ through time-series, $i = 1, \dots, N$.
Transport $p_{0,sub}^{(i)}, i = 1, \dots, N$ into population template using Eqn. (8) and average:

$$\bar{p}_0 = \frac{1}{N} \sum_{i=1}^N D\Phi^{(i)}([\Phi^{(i)}]^{-1})^T p_{0,sub}^{(i)}([\Phi^{(i)}]^{-1}).$$

Generate population infinitesimal mean μ solving conservation laws from \bar{p}_0 .

Coadjoint transport template-space initial momentum into subject i coordinate space:

$$\bar{p}_{0,sub}^{(i)} = D[\Phi^{(i)}]^{-1}(\Phi^{(i)})^T \bar{p}_0(\Phi^{(i)}).$$

Generate mean flow in subject-specific coordinates for each subject $i = 1, \dots, N$ from initial conditions $\bar{p}_0^{(i)}$:

$$\frac{d}{dt} \bar{p}_t^{(i)} = -d(\mu_t^{(i)})^T \bar{p}_t^{(i)}, \text{ i.c. } p_0^{(i)} \quad (9a)$$

$$\mu_t^{(i)} = \int K(\cdot, \varphi_t^{(i)}(x)) \bar{p}_t^{(i)}(x) dx. \quad (9b)$$

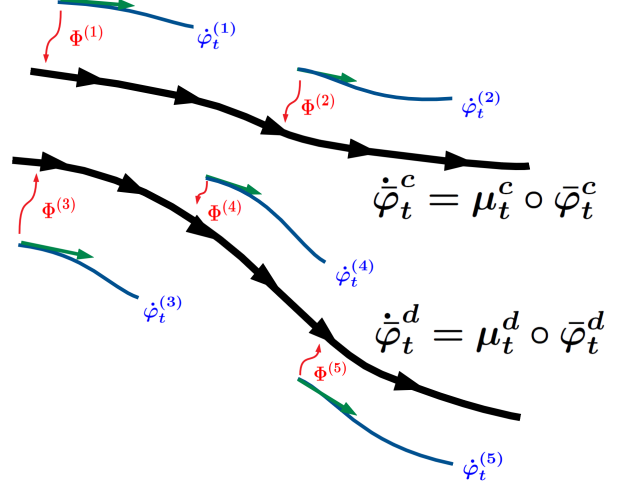


Figure 2. Estimating mean drifts associated to two subpopulations of surfaces corresponding to labeled subjects forming the control (μ^c) and disease (μ^d) subgroups where subjects 1 & 2 belong to the control group and subjects 3-5 belong to the MCI group.

3. Experiments

3.1. Simulations based on Geodesic Shooting

We first apply our proposed model to simulated triangulated surface data. Illustrated in Figure 3, a disc-like surface and a cube-like surface are observed deforming over time by their own subject specific trajectories parameterized by $p_{0,sub}^{(i)}$. Each $p_{0,sub}^{(i)}$ is transported into the template coordinate space where the template is represented by a sphere. Here, the momenta are averaged, producing \bar{p}_0 (purple vectors), the momentum parameterizing the mean drift. For simplicity, we show simulated data that are synchronized in time by their baseline observations with surface triangulations that have corresponding vertices.

Figure 4 shows examples of subject-specific deviations from the simulated drift of Figure 3. In this example, a pyramid-like subject changes longitudinally by expanding in the horizontal plane along an axis between two corners of the pyramid. The drift \bar{p}_0 can be transported into the space of this subject, producing $\bar{p}_{0,sub}^{(i)}$ (shown in purple vectors on the pyramid). The method described in (6) is used to compute the personalized control, shown in the bottom row. Naturally, because the pyramid expands from corner to corner with no change in any other direction while the drift expands in all directions, the resulting personalized control shows sharp expansion from corner to corner and shrinkage in all other directions. Shrinkage of a surface can be measured by several metrics. We choose to examine the log determinant of the jacobian of the deformation of the transported template surface in directions tangent to the surface, hereafter referred to as the "surface atrophy measure".

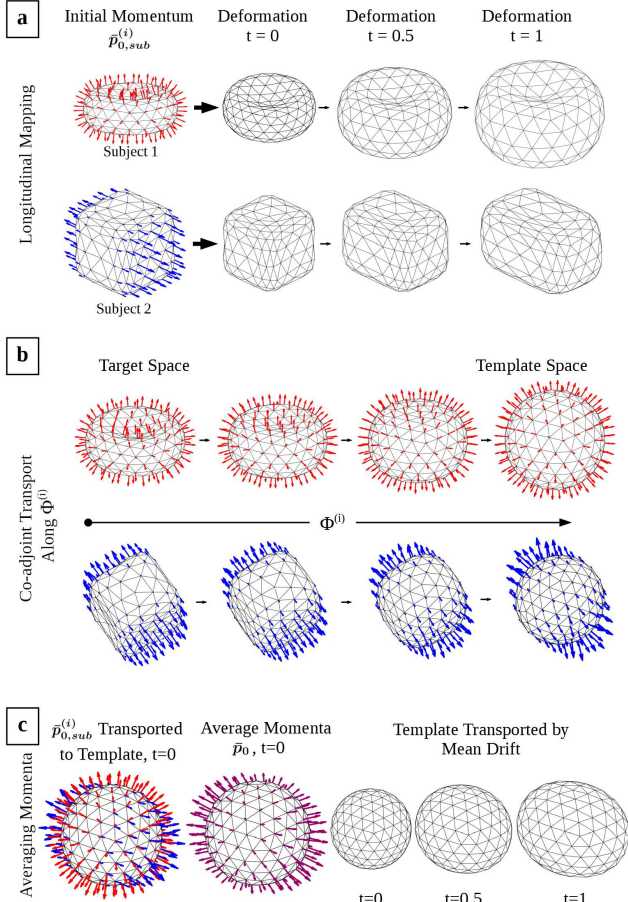


Figure 3. Longitudinal LDDMM shooting on simulated data computes the independent subject trajectories parameterized by initial momentum $p_{0,sub}^{(i)}$ shown as red and blue vectors in the left column of panel (a). The subject surface at time 0 is transported by $p_{0,sub}^{(i)}$, following the rightwards arrows for two subjects in panel (a) where subject 1 uniformly expands and subject 2 expands along a single axis. Panel (b) shows the initial momenta $p_{0,sub}^{(i)}$ transported into the template coordinate space by coadjoint transport along $\Phi^{(i)}$ for both subjects, where the template is chosen as a sphere. The transported momenta are averaged in template space in panel (c) to produce \bar{p}_0 in purple and the template surface is shown being transported by the mean drift resulting from \bar{p}_0 .

3.2. Alzheimer's Disease Neuroimaging Initiative

We apply our model to neuroimaging data from the Alzheimer's Disease Neuroimaging Initiative dataset, a longitudinal imaging study of neurodegeneration in a patient population at risk for Alzheimer's. The dataset contains 3T MRI scans for 57 patients (22 controls and 35 diagnosed mild cognitive impairment [MCI]) over the course of two years with intervals at baseline, 6 months, 12 months, and 24 months; the patient cohorts have been examined by multiple prior studies. We extend our model to study the drift

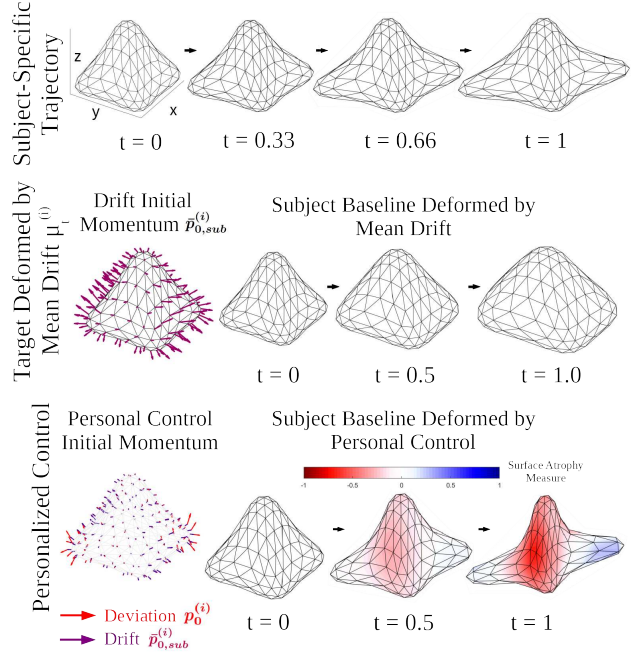


Figure 4. Personalized controls are shown for a simulated surface from the mean drift of Figure 3. The top row shows an individual subject's longitudinal trajectory, in which a pyramid-like surface expands in one direction across two corners. The middle row shows the initial momentum parameterizing the mean drift $\mu_t^{(i)}$ in purple arrows (transported into the subject coordinate space) of Figure 3 and the baseline ($t = 0$) subject surface deformed by the flow resulting from the transported drift. The bottom left panel shows $p_0^{(i)}$ computed for this subject, the initial momentum parameterizing $w_t^{(i)}$, computed by (6). The panels to the right show the subject baseline surface deformed by the flow resulting from $w_t^{(i)}$ overlayed with the surface atrophy measure associated with the personalized control where red indicates shrinkage tangent to the surface.

of two populations as illustrated in Figure 2.

For simplicity of demonstration we choose to chronologically synchronize all subjects to their baseline scan date, however we note the proposed framework is suitable for any arbitrary synchronization with no requirement for corresponding baseline scan times. We then demonstrate the computation of the deviation of MCI patient group members from the mean drift of the normal population.

3.3. Surface Representation of Subcortical Structures in ADNI

We choose to examine longitudinal shape changes in the entorhinal and transentorhinal cortex (hereafter referred to as the entorhinal cortex) of the brain, a region which has previously been linked to Alzheimer's Disease. Figure 5 illustrates the process of seeding triangulated surfaces onto the combination of these regions in MR. Manual voxel-wise

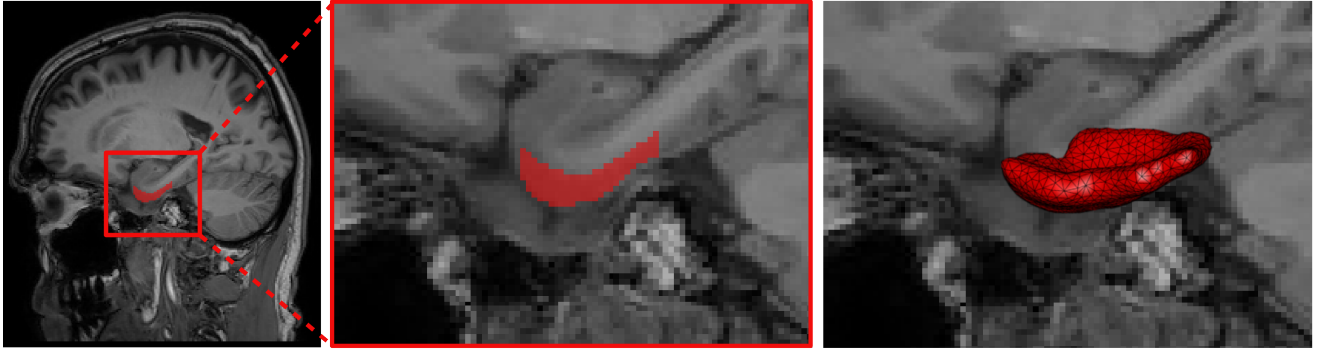


Figure 5. Surface generation process. (left) Sagittal view of 3T brain MRI in a section passing through the entorhinal cortex. (middle) Manual voxel-wise segmentations of the entorhinal and transentorhinal cortex are performed by anatomical experts. (right) Smooth triangulated surfaces are seeded on the segmentations.

binary segmentations of the entorhinal cortex were performed by anatomists and these segmentations were used to build smooth triangulated surfaces for each subject at every time point.

3.4. Computing the Drift of ADNI Populations

Bayesian template estimation [27] was performed on baseline surfaces for the 57 subjects in order to build a template coordinate space at the baseline timepoint ($t=0$). The

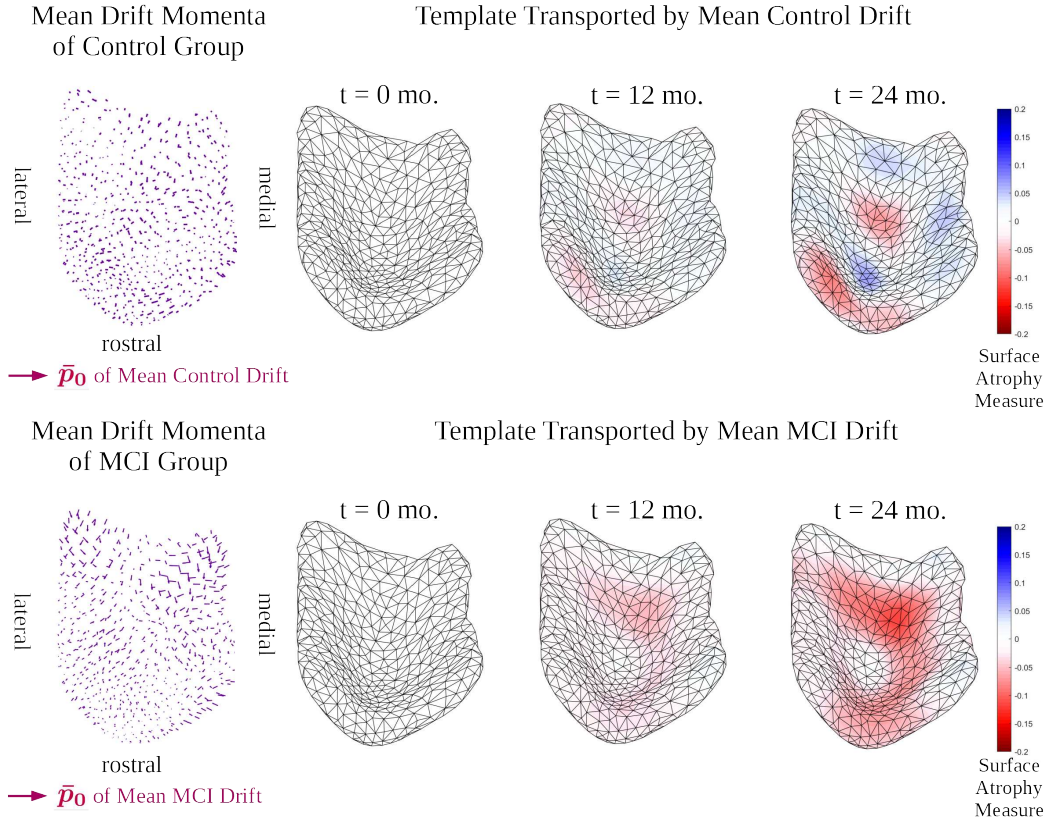


Figure 6. Population mean drift of ADNI patient cohort separated by control group and MCI group. The left column displays initial momentum vectors at each vertex of the template surface parameterizing the mean drift of each population. The right columns show the template surface deformed by the resulting flow of each population drift, sampled at baseline, one year, and two years. The surface atrophy measure is plotted on the flowing surfaces where red represents shrinkage tangent to the surface and blue represents expansion.

template surface T was mapped to each subject baseline using diffeomorphic surface matching with data attachment term based on currents [44], producing the transform $\Phi^{(i)}$ for $i \in 1, 2, \dots, 57$. Then, at each baseline timepoint for each subject, we have $\Phi^{(i)} \cdot T$ which is mapped longitudinally through each subject's subsequent surfaces in a single trajectory which minimizes the sum of currents between the deformed template and the subject's triangulated surface at each time point, producing $p_{0,sub}^{(i)}$ for $i \in 1, 2, \dots, 57$.

The initial momenta $p_{0,sub}^{(i)}$ parameterizing each independent subject specific trajectory are then transported into the template space using coadjoint transport and averaged to produce the population drift. We produce two population drifts: 1) the 22 control subjects who did not develop MCI and 2) the 35 subjects who did develop MCI.

In order to visualize the mean flow of each population, we transport the template surface along each computed drift. Snapshots of the deformed template sampled at selected time points along the continuous drift trajectory are shown in Figure 6 with each surface face colored by the log

determinant of jacobian of the drift deformation tangent to the surface (where red indicates shrinkage).

As expected, the mean drift of the control population fluctuates around identity. On the other hand, the mean drift of the MCI population shows obvious atrophy as evidenced by the red region in the bottom row of Figure 6. Measurements on our transported templates showed 1.6% volume loss in the control population and 8.3% volume loss in the MCI population. These values are in line with previous studies of entorhinal cortex atrophy in Alzheimer's Disease [43] and notably, the atrophy pattern measured by the drift qualitatively matches that observed in those studies.

3.5. Computing the Personalized Controls of ADNI Subjects

Having computed the drift of populations in the dataset, we can now apply our new biased geodesic shooting algorithm to compute the deviation or personalized control of individuals from the mean drift. For understanding biomarkers of Alzheimer's Disease and dementia, we are interested in examining the deviation of entorhinal cortex atrophy of

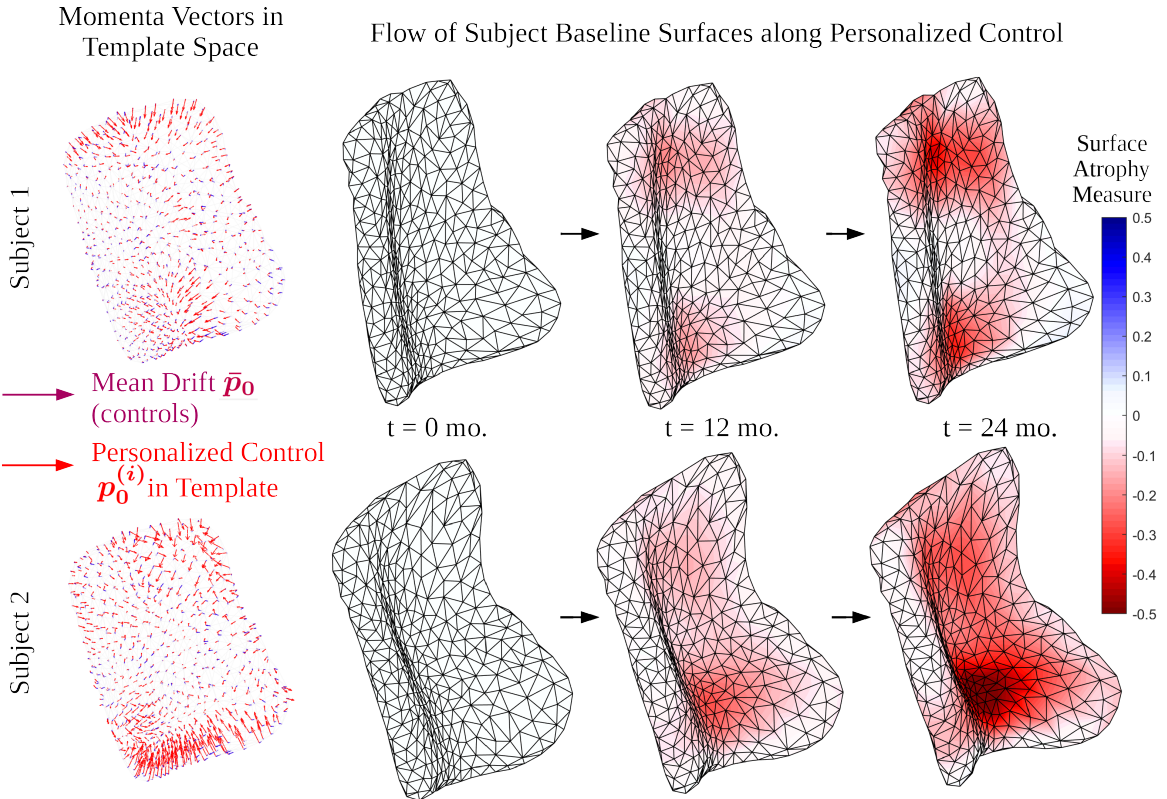


Figure 7. Personalized controls for two selected subjects from the MCI patient group. The left column shows the mean control population drift initial momentum \bar{p}_0 (in purple vectors, scaled linearly for visibility) along with the additional deviation computed to match the subject-specific observations $p_0^{(i)}$ transported to template space (in red vectors, scaled by the same linear factor). The right column shows the baseline surface of each subject deformed by the flow resulting from the personalized control only. The surface atrophy measure is plotted on the flowing surfaces where red represents shrinkage and blue represents expansion.

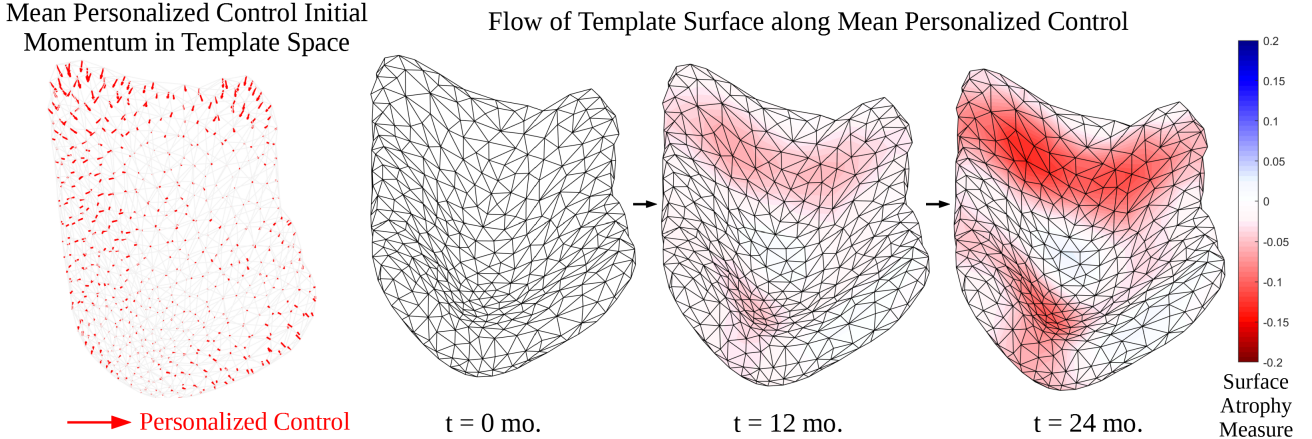


Figure 8. Mean personalized control parameterized by initial momentum vectors are shown in the left column. The template flowed along the trajectory defined by the mean personalized control is shown to the right, overlayed with the surface atrophy measure where red represents shrinkage.

patients in the MCI group from the mean drift of the control group. This would inform us about the additional deformation imposed on each subject's entorhinal cortex on top of the shape change associated with normal aging.

We apply the model of (4) in order to compute the personalized control of each individual. First, we transport the drift into the coordinate space of the subject. Since the drift is specified by the initial momentum \bar{p}_0 in our case, we coadjointly transport \bar{p}_0 into each subject coordinate space to obtain $\bar{p}_{0,sub}^{(i)}$. From there we apply Eqn (6) to compute $w_t^{(i)}$ for each subject. Figure 7 shows two sample deviations from the drift of the MCI patient population overlayed with the surface atrophy measurement at selected time intervals.

In order to summarize the individual deviations for the entire population, we compute the individual deviations for all 37 subjects in the MCI patient group, as described above. The initial momenta parameterizing the flows associated to their personalized controls are then coadjointly transported back into the template space and averaged using the same method of Algorithm 1. The resulting flow describes the average deviation in the shape of the entorhinal cortex of MCI patients from the mean drift characterizing the normal population. Figure 8 shows this mean deviation sampled at several time points. As expected, we generally observe a trend towards shrinkage of the entorhinal cortex in MCI patients away from the normal population drift. Our model shows precisely where this deviation occurs in specific patients as well as on the average.

4. Conclusion

In this paper we have introduced a new method for computing biased geodesics that describe deviations of

subject-specific longitudinal trajectories, or "personalized controls", from a given drift. We have described the dynamical systems framework that governs our model as well as an algorithm to solve for the personalized controls. We solve the control problem of mapping a template onto members of a population using surface matching of triangulated meshes onto targets. This method can be generalized to include volumes or landmarks, as well as to simultaneously optimize the mean flow along with each individual's personal flow. We emphasize that there is no penalty on the drift generated from the population as we assume the drift is of dimension consistent with that of the population from which it was estimated. Our algorithm treats the mean drift as having no metric cost like identity, and as a result, deviations from that drift are more naturally penalized. For this reason, we use LDDMM shooting onto the population to control the initial dimensions of the mean drift as the order of the database is limited. In our experiments on entorhinal cortical surfaces from the ADNI dataset, we show that we are able to compute a realistic mean drift of two diagnostic groups within the patient cohort under our model, and that we are able to compute the deviations of MCI group individuals from the normal population drift as well as compute the mean deviation in a common coordinate space.

Acknowledgements

This work was supported by the NIH (P41-EB-015909, R01-EB-020062, U19-AG-033655), NSF (ACI1548562 via XSEDE), and Kavli Neuroscience Discovery Institute. MIM reports personal fees from AnatomyWorks, LLC, outside the submitted work, and jointly owns AnatomyWorks. MIM's relationship with AnatomyWorks is being handled under full disclosure by the Johns Hopkins University.

References

- [1] John Ashburner. Computational anatomy with the spm software. *Magnetic Resonance Imaging*, 27:1163–1174, October 2009.
- [2] John Ashburner and Karl J. Friston. Computational anatomy. In K J Friston, J Ashburner, S J Kiebel, T E Nichols, and W D Penny, editors, *Statistical Parametric Mapping The Analysis of Functional Brain Images*, pages 49–100. Academic Press, 2007.
- [3] Lalit Bahl, Frederick Jelinek, and Robert Mercer. A maximum likelihood approach to continuous speech recognition. *Pattern Analysis and Machine Intelligence, IEEE Transactions on*, PAMI-5:179 – 190, 04 1983.
- [4] Alexandre Bône, Olivier Colliot, and Stanley Durrleman. Learning the spatiotemporal variability in longitudinal shape data sets, 2019. HAL Preprint: fhal-02091549v4f.
- [5] Alexandre Bône, Maxime Louis, Benoît Martin, and Stanley Durrleman. Deformetrica 4: an open-source software for statisticalshape analysis. In *ShapeMI @ MICCAI 2018, Lecture Notes in Computer Science*, volume 11167, 2018.
- [6] Jan M. Van Campenhout and T. M. Cover. Maximum entropy and conditional probability. *IEEE Transactions on Information Theory*, IT-27, No. 4:483–489, July 1981.
- [7] Gary E. Christensen, Sarang C. Joshi, and Michael I. Miller. Volumetric transformation of brain anatomy. *IEEE TRANSACTIONS ON MEDICAL IMAGING*, 16(6):864–877, 1997.
- [8] Ronald R. Coifman and Mladen .V. Wickerhauser. Entropy based algorithms for best basis selections. *IEEE Trans. on Information Theory*, 38:713–718, 1992.
- [9] John Csernansky, Mathew Schindler, N Splinter, Lei Wang, Mohktar Gado, Lynn Selemion, Devna Rastogi-Cruz, Joel Posener, Paul Thompson, and Michael Miller. Abnormalities of thalamic volume and shape in schizophrenia. *The American journal of psychiatry*, 161:896–902, 06 2004.
- [10] J.G. Csernansky, Lei Wang, Swank JS, J. Miller, Mohamed Gado, Dan McKeel, M Miller, and John Morris. Preclinical detection of alzheimer’s disease: Hippocampal shape and volume predict dementia onset in the elderly. *NeuroImage*, 25:783–92, 05 2005.
- [11] John G. Csernansky, Lei Wang, D. Kido, Mohktar Gado, John C. Morris, and Michael I. Miller. Hippocampal morphometry in dementia of the alzheimer type by computer algorithm. *Soc Neurosci Abst*, (24):264, 1998.
- [12] Paul Dupuis, Ulf Grenander, and Michael I Miller. Variation Problems on Flows of Diffeomorphisms for Image Matching. *Quarterly of Applied Mathematics*, LVI(4):587–600, 1998.
- [13] Stanley Durrleman, Pierre Fillard, Xavier Pennec, Alain Trouvé, and Nicholas Ayache. Registration, atlas estimation and variability analysis of white matter fiber bundles modeled as currents. *NeuroImage*, 55(3):1073–1090, 2011.
- [14] Stanley Durrleman, Xavier Pennec, Jose Braga Alain Trouve, Guido Gerig, and Nicholas Ayache. Toward a comprehensive framework for the spatiotemporal statistical analysis of longitudinal shape data. *Int J Comp Vis*, 103(1):22–59, 2013.
- [15] Stuart Geman and Donald Geman. Stochastic relaxation, gibbs distributions, and the bayesian restoration of images. *IEEE Trans. Pattern Anal. Machine Int.*, 6:721–741, 1984.
- [16] Stuart Geman and Chii Ruey Hwang. Diffusions for global optimization. *SIAM J. Control and Optimization*, 24:1031–1043, 1987.
- [17] B. Gidas. Global optimization via the langevin equation. In *Proceedings of the 24th Conference on Decision and Control*, pages 774–778, Ft. Lauderdale, Fl., December 1985.
- [18] Ulf Grenander and Michael I. Miller. Representations of knowledge in complex systems. *J. Roy. Stat. Soc. B*, 56(3):549–603, 1994.
- [19] Ulf Grenander and Michael I. Miller. Computational anatomy: An emerging discipline. *Quarterly of Applied Mathematics*, 56(4):617–694, 1998.
- [20] Darryl D. Holm. Variational principles for stochastic fluid dynamics. *Proceedings of the Royal Society A: Mathematical, Physical and Engineering Sciences*, 471(2176):20140963, Apr 2015.
- [21] E.T. Jaynes. On the rationale of maximum-entropy methods. *Proc. of the IEEE*, 70:939–952, September 1982.
- [22] R.W. Johnson, J.E. Shore, and J.P. Burg. Multisignal minimum-cross-entropy spectrum analysis with weighted initial estimates. *IEEE Transactions on Acoustics, Speech and Signal Processing*, ASSP-32, No.3:531–539, June 1984.
- [23] SC Joshi and MI Miller. Landmark matching via large deformation diffeomorphisms. *IEEE Trans Image Process*, 9(8):1357–70, 2000.
- [24] Samuel Karlin and Howard Taylor. In *Second Edition: A First Course in Stochastic Processes*, pages 1–557. Academic Press, December 2012.
- [25] Marco Lorenzi, Nicholas Ayache, Giovanni B Frisoni, and Xavier Pennec. Mapping the effects of ab1-42 levels on the longitudinal changes in healthy aging: Hierarchical modeling based on stationary velocity fields. In *Medical Image Computing and Computer-Assisted Intervention – MICCAI 2011.*, volume 6892, Berlin, Heidelberg, 2011. Springer.
- [26] Marco Lorenzi, Xavier Pennec, Giovanni Frisoni, and Nicholas Ayache. Disentangling normal aging from alzheimer’s disease in structural mr images. *Neurobiology of aging*, 36, 2015.
- [27] Jun Ma, Michael I Miller, Alain Trouvé, and Laurent Younes. Bayesian template estimation in computational anatomy. *NeuroImage*, 42(1):252–261, 2008.
- [28] Michael Miller, Sylvain Arguillere, Daniel Tward, and Laurent Younes. Computational anatomy and diffeomorphometry: A dynamical systems model of neuroanatomy in the soft condensed matter continuum. *Wiley Interdiscip Rev Syst Biol Med*, 10(6), 2018.
- [29] M.I. Miller and D.L. Snyder. The role of likelihood and entropy in incomplete-data problems: Applications to estimating point-process intensities and toeplitz constrained covariances. *Proceedings of the IEEE*, 75, No.7:892–907, July 1987.
- [30] Michael Miller, Laurent Younes, John Ratnanather, Timothy Brown, Huong Trinh, Elizabeth Postell, David Lee, Meicheng Wang, Susumu Mori, Richard O’Brien, and Marilyn

- Albert. The diffeomorphometry of temporal lobe structures in preclinical alzheimer's disease. *NeuroImage: Clinical*, 3:352–360, 12 2013.
- [31] Michael I. Miller. Computational anatomy: shape, growth, and atrophy comparison via diffeomorphisms. *Neuroimage*, 29(Suppl 1:S):19–33, 2004.
- [32] Michael I. Miller, Alain Trouvé, and Laurent Younes. Geodesic shooting for computational anatomy. *J. Mathematical Imaging and Vision*, 24:209–228, 2006.
- [33] Michael I. Miller, Alain Trouvé, and Laurent Younes. Hamiltonian systems and optimal control in computational anatomy: 100 years since d'arcy thompson. *Annual Review of Biomed Engineering*, (17):447–509, November 4 2015.
- [34] Ronald Petersen, P.S. Aisen, L.A. Beckett, Michael Donohue, A.C. Gamst, D.J. Harvey, Clifford Jack, W.J. Jagust, Leslie Shaw, A.W. Toga, J.Q. Trojanowski, and Michael Weiner. Alzheimer's disease neuroimaging initiative (adni): Clinical characterization. *Neurology*, 74:201–9, 01 2010.
- [35] Anqi Qiu, Deana Crocetti, Marcy Adler, E Mahone, Martha Denckla, Michael Miller, and Stewart Mostofsky. Basal ganglia volume and shape in children with attention deficit hyperactivity disorder. 166:74–82, 12 2008.
- [36] Anqi Qiu and Michael I. Miller. Multi-structure network shape analysis via normal surface momentum maps. *NeuroImage*, 42(4):1430 – 1438, 2008.
- [37] Anqi Qiu, Christine Fennema Notestine, Anders M. Dale, Michael I. Miller, and Alzheimers Disease Neuroimaging Initiative. Regional subcortical shape abnormalities in mild cognitive impairment and alzheimer's disease. *NeuroImage*, 45:656–661, 2009.
- [38] Anqi Qiu, Marc Vaillant, Patrick Bartay, J. Tilak Rantanather, and Michael I. Miller. Region of interest based analysis of cortical thickness variation of left planum temporale in schizophrenia and psychotic bipolar disorder. *Human Brain Mapping*, 29:973–985, 2008.
- [39] Raphaël Sivera, Hervé Delingette, Marco Lorenzi, Xavier Pennec, and Nicholas Ayache. A model of brain morphological changes related to aging and alzheimer's disease from cross-sectional assessments. *NeuroImage*, 198, 05 2019.
- [40] Xiaoying Tang, Dominic Holland, Anders Dale, Laurent Younes, and Michael Miller. The diffeomorphometry of regional shape change rates and its relevance to cognitive deterioration in mild cognitive impairment and alzheimer's disease: Diffeomorphometry of regional shape change rates. *Human Brain Mapping*, 36(6):2093–2117, 2015.
- [41] Alain Trouvé. Action de groupe de dimension infinie et reconnaissance de formes. *C R Acad Sci Paris Sér I Math*, 321(8):1031–1034, 1995.
- [42] Daniel J Tward, Michael I Miller, Alain Trouve, and Laurent Younes. Parametric surface diffeomorphometry for low dimensional embeddings of dense segmentations and imagery. *IEEE Transactions on Pattern Analysis and Machine Intelligence*, PP(99), 2016.
- [43] Daniel J Tward, Chelsea S. Sicat, Timothy Brown, Arnold Bakker, Michela Gallagher, Marilyn Albert, and Michael Miller. Entorhinal and transentorhinal atrophy in mild cognitive impairment using longitudinal diffeomorphometry. *Alzheimers Dement*, 9:41–50, 2017.
- [44] Marc Vaillant and Joan Glaunès. Surface matching via currents. In *Proceedings of Information Processing in Medical Imaging (IPMI 2005)*, number 3565 in *Lecture Notes in Computer Science*, pages 381–392, 2005.
- [45] Lei Wang, J. Miller, Mokhtar Gado, Dan McKeel, Marcus Rothermich, Michael Miller, John Morris, and John Csernansky. Abnormalities of hippocampal surface structure in very mild dementia of the alzheimer type. *NeuroImage*, 30:52–60, 04 2006.
- [46] Lei Wang, J. Philip Miller, Mokhtar H. Gado, Daniel McKeel, Michael I. Miller, John C. Morris, and John G. Csernansky. Hippocampal shape abnormalities in early ad: A replication study. In *Alzheimer's Association International Conference on Prevention of Dementia: Early Diagnosis and Intervention*, Washington, D.C., 2005.
- [47] L. Wang, J. S. Swank, I. E. Glick, M. H. Gado, M. I. Miller, J. C. Morris, and J. G. Csernansky. Changes in hippocampal volume and shape across time distinguish dementia of the alzheimer type from healthy aging. *Neuroimage*, 20:667–82, 2003.
- [48] Laurent Younes, John Ratnanather, Timothy Brown, Elizabeth Aylward, Peg Nopoulos, Hans Johnson, Vincent Magnotta, Jane Paulsen, Russell Margolis, Roger Albin, Michael Miller, and Christopher Ross. Regionally selective atrophy of subcortical structures in prodromal hd as revealed by statistical shape analysis. *Human brain mapping*, 35, 03 2014.
- [49] Song Zhu, Yingnian Wu, and David Mumford. Minimax entropy principle and its application to texture modeling. *Neural Computation*, 9, 09 2000.